A numerical fractional flow model for air sparging

EINDHOVEN UNIVERSITY OF TECHNOLOGY
Department of Mathematics and Computing Science

RANA 97-11
September 1997

A Numerical Fractional Flow Model for Air Sparging

by

E.F. Kaasschieter
J.D. van der Werff ten Bosch
G.J. Mulder

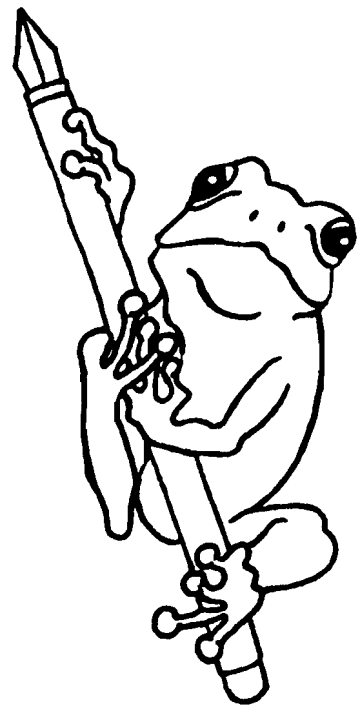

Reports on Applied and Numerical Analysis
Department of Mathematics and Computing Science
Eindhoven University of Technology
P.O. Box 513
5600 MB Eindhoven
The Netherlands
ISSN: 0926–4507

A Numerical Fractional Flow Model for Air Sparging

E.F. Kaasschieter
Department of Mathematics and Computing Science,
Eindhoven University of Technology,
P.O. Box 513, 5600 MB Eindhoven, The Netherlands
wsanrk@win.tue.nl

J.D. van der Werff ten Bosch
Resource Analysis,
Zuiderstraat 110, 2611 SJ Delft, The Netherlands
jasper.v.d.werff@resource.nl

G.J. Mulder
Delft Geotechnics,
P.O. Box 69, 2600 AB Delft, The Netherlands
g.j.mulder@delftgeot.nl

Abstract

Spillage of organic compounds into the subsurface environment can result in costly remediation. As a possibly effective remediation technique, the injection of air into the groundwater (air sparging) has recently gained significant attention. The injected air migrates towards the unsaturated zone, volatising contaminants from the groundwater and delivering oxygen to biota for biodegradation.
This article concerns the applicability of some numerical schemes for the two-phase flow process. The flow turns out to be predominantly driven by convection. It is modelled using a fractional flow approach, which yields a quasi-hyperbolic governing equation for the air saturation. It appears that this equation can be solved effectively by suitable modifications of explicit conservative schemes for hyperbolic conservation laws. A first order Godunov method and a high resolution method are considered as examples. Results are presented and discussed for flow in a homogeneous isotropic medium, both for a one-dimensional as a multi-dimensional case.

Keywords: air sparging, fractional flow, Godunov scheme, high resolution scheme.

1 Introduction

Accidental releases of organic compounds into the subsurface environment in the form of petroleum products or industrial solvents can result in costly remediation.
As a cost-effective in-situ remediation technique, the injection of air into groundwater (air sparging) has gained significant attention since the mid eighties. A typical air sparging system has one or more subsurface wells through which air is injected. The injected air migrates towards the unsaturated zone, volatising contaminants from the groundwater and delivering oxygen to biota for in-situ biodegradation. The contaminated vapours are typically extracted from the unsaturated zone with a soil extraction system. Relevant topics for the effective application of air sparging include soil layering and heterogeneity, air flow patterns and the concepts of radius of influence and rate of remediation. Numerous accounts describing applications of the technique on both field and laboratory scale have been presented in the literature, as well as attempts to capture the various air sparging phenomena in mathematical models. An overview of recent developments considering a wide range of aspects of air sparging can be found in [6].
In this article we will focus on the numerical treatment of the two-phase flow of air and water. The two phases will be considered as two immiscible incompressible continuous phases, both obeying Darcy's law. Air-saturation dependent permeability and capillary pressure relations describe the interaction between the phases and the porous medium.
In Section 2 the basic equations are given for a homogeneous isotropic porous medium in a three-dimensional setting. Two approaches for the modelling of the flow are considered, i.e. the commonly used mixed form of Richards equation and the so-called fractional flow model. In Section 3 the fractional flow model is considered in a simple one-dimensional setting. The governing equation for air saturation is found to be quasi-hyperbolic due to a dominating convective component. Modifications of the first order Godunov scheme and a high resolution scheme are evaluated for the numerical solution of the one-dimensional problem. In Section 4 a typical multi-dimensional case is considered. The fluid pressure is computed by a finite volume method. Some conclusions are listed in the final section.

2 Statement of the model

2.1 Governing equations

In this section a general mathematical model is presented for air sparging. Air sparging is a three-dimensional two-phase flow process of air and water, starting in the saturated zone of a porous medium and passing to the unsaturated zone.
It is assumed that the flow of both air and water can be adequately described by Darcy's law. If the phases are immiscible, then the following equations are representative in a Cartesian coordinate system for which the gravitational force points in the same direction as the negative z-axis:

$$\frac{\partial(\phi\rho_l S_l)}{\partial t} + \nabla\cdot(\rho_l \mathbf{v}_l) = 0,\ l = a, w, \tag{1}$$

$$\mathbf{v}_l = -\mathbf{K}\frac{k_l}{\mu_l}\nabla(p_l + \rho_l g z),\ l = a, w. \tag{2}$$

Equation (1) expresses conservation of mass. Herein, ϕ [−] denotes the porosity while ρ_l [kg m^{-3}], S_l [−] and $\mathbf{v}_l$ [m s^{-1}] respectively denote fluid density, saturation and specific discharge. The specific discharge is given by Darcy's law, i.e. (2), in which p_l [Pa], μ_l [Pa s], k_l [−] are the fluid pressure, viscosity and relative permeability. Clearly, the index l can either be a (air phase) or w (water phase). Also in (2), we have g [m s^{-2}] denoting the acceleration due to gravity and $\mathbf{K}$ [m^2] the absolute permeability tensor. The two phases are linked by the identity $S_a + S_w = 1$. With the above expressions in the three-dimensional case, for each phase we have four equations and six unknowns: ρ_l, S_l, $v_{x,l}$, $v_{y,l}$, $v_{z,l}$ and p_l. Later on it will be shown how the system can be closed using additional constitutive relations.

2.2 Simplified equations

In this study, a homogeneous isotropic medium is considered, i.e. the porosity and absolute permeability are assumed to be constant and uniform whilst the tensor $\mathbf{K}$ reduces to a scalar K.

With respect to the flow, both phases are assumed to have constant and uniform viscosity, and to be incompressible. Especially for the air phase, the latter assumption seems to be a quite rigorous one as it is intuitively clear that air rising from an air sparging well to the surface will undergo changes in density. However, considering the hydrostatic pressure at depths of about 5 m (at which air is usually injected) and the fact that air-sparging entry pressures do generally not exceed the local water pressure by much, it seems reasonable to disregard variations in air density.

With these assumptions, (1) and (2) change into

$$\phi\frac{\partial S_l}{\partial t} + \nabla \cdot \mathbf{v}_l = 0,\ l = a, w. \tag{3}$$

$$\mathbf{v}_l = -\frac{K k_l}{\mu_l}(\nabla p_l + \rho_l g \mathbf{e}_z),\ l = a, w, \tag{4}$$

where $\mathbf{e}_z$ is the unit vector in the positive z-direction.

2.3 Completing the flow model

In order to solve the flow problem (3)–(4), it is necessary to close the system. This can be done by the use of constitutive relations linking pressure, saturation and relative permeability. First we scale saturation and porosity to obtain effective saturation and effective porosity:

$$S_w^* = \frac{S_w - S_r}{1 - S_r},\ S_a^* = \frac{S_a}{1 - S_r},\ \phi^* = (1 - S_r)\phi,$$

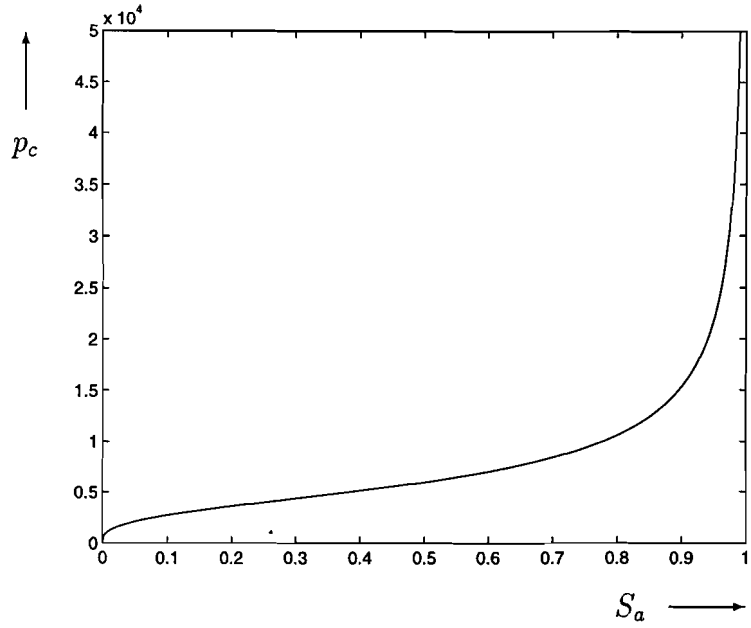

Figure 1: Typical capillary pressure curve

where S_r denotes the residual water saturation. Having scaled these variables, we omit the stars. The following empirical relations are currently widely used to describe how capillary pressure and relative permeability in a two-phase system depend on saturation (see [3], [9] and [2]):

$$\left.\begin{aligned} p_c(S_a) &= p_a - p_w = \frac{(\rho_w - \rho_a)g}{\alpha}\left((1-S_a)^{-1/m}-1\right)^{1-m}, \\ k_w(S_w) &= S_w^{1/2}\left(1-\left(1-S_w^{1/m}\right)^m\right)^2, \\ k_a(S_a) &= S_a^{1/2}\left(1-(1-S_a)^{1/m}\right)^{2m}, \end{aligned}\right\} \tag{5}$$

where m [–] and α [m^{-1}] are empirical soil parameters satisfying $0 < m < 1$ and $\alpha > 0$. Not included in (5) is the phenomenon of hysteresis. Hysteresis explains why, as soil is wetted, the yielded (empirical) capillary pressure and relative permeability curves are different compared to the reverse situation when the soil is drained. Hysteresis can have a significant effect on flow behaviour in case the soil is alternately wetted and drained. As in the case of air sparging the soil is primarily drained, however, the effect is not believed to play an important role and is therefore disregarded.

It can be easily seen that the above relations possess common features of pressure and permeability curves, such as $p_c(0) = 0$, $k_l(0) = 0$, $k_l(1) = 1$, p_c tending to infinity as S_a tends to one and p_c having a vertical tangent at $S_a = 0$. As hysteresis is not considered, all relations are reversible. Typical examples of capillary pressure and relative permeability curves can be seen in Figures 1 and 2 for $m = 2/3$ and $\alpha = 2\ \mathrm{m}^{-1}$.

For a three-dimensional domain, the flow system considered consists of ten unknowns $\mathbf{v}_l$, S_l and p_l, with $l = a, w$. Equations (3) and (4) are two mass conservation equations and

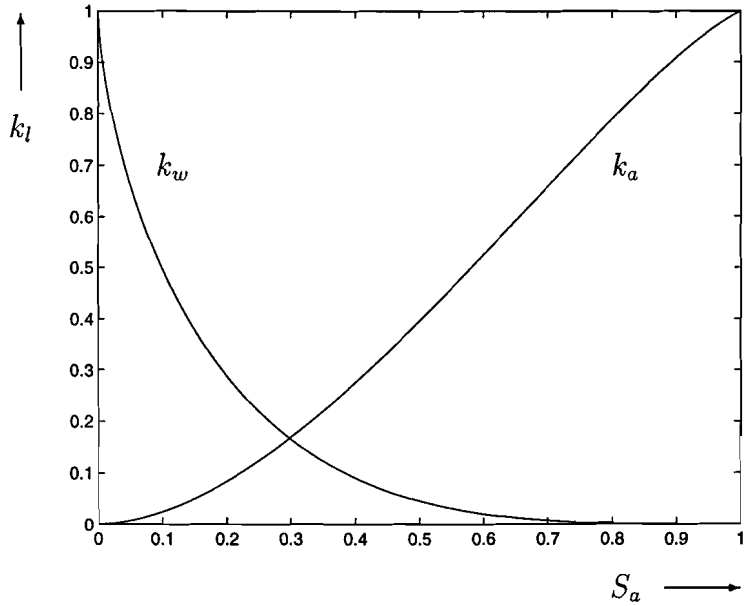

Figure 2: Typical relative permeability curves

six equations of motion (Darcy). The remaining two equations are provided by the identity $S_a + S_w = 1$ and by the capillary pressure relation of (5). These equations also provide expressions for the relative permeability, necessary for the solution of the equations of motion. Thus, we have a closed system which is referred to as the mixed form of Richards equation (see [2]).

2.4 The fractional flow model

A formulation that is often used for multi-phase flow problems is the so-called fractional flow model. It is equivalent to (3) and (4) and yields two separate equations for saturation and specific discharge. One of the major advantages of this formulation is that the model becomes more accessible to analysis. For our purposes the use is evident as will be explained in the next section.
Adding the equations (4) for both phases and using the identity $S_a + S_w = 1$ we obtain

$$\nabla \cdot \mathbf{v}_t = 0, \tag{6}$$

in which $\mathbf{v}_t = \mathbf{v}_a + \mathbf{v}_w$ is the total specific discharge. Equation (6) expresses conservation of mass. To obtain the equation for air saturation (from which water saturation is immediately found from $S_w = 1 - S_a$), (4) is rewritten as

$$\nabla p_l = -\frac{\mathbf{v}_l}{\lambda_l} - \rho_l g \mathbf{e}_z, \; l = a, w, \tag{7}$$

where the mobility of phase l, λ_l [$\mathrm{m^2\ Pa^{-1}\ s^{-1}}$], is defined as

$$\lambda_l = \frac{K k_l}{\mu_l}, \; l = a, w.$$

We subtract (7), $l = w$, from (7), $l = a$, to obtain

$$\nabla p_c = -\frac{\mathbf{v}_a}{\lambda_a} + \frac{\mathbf{v}_w}{\lambda_w} + (\rho_w - \rho_a) g \mathbf{e}_z.$$

With $\mathbf{v}_w = \mathbf{v}_t - \mathbf{v}_a$ this can be written as

$$\mathbf{v}_a = f_a[\mathbf{v}_t + \lambda_w((\rho_w - \rho_a) g \mathbf{e}_z - \nabla p_c)],$$

where the *air fractional flow* function f_a [–] is defined by

$$f_a = \frac{\lambda_a}{\lambda_a + \lambda_w}.$$

In the above, f_a, λ_w, and p_c are non-linear functions of S_a, directly available from the Van Genuchten constitutive relations (5).
The systems (3) and (4) can now be rewritten in terms of air saturation and total Darcy velocity:

$$\left.\begin{aligned} &\phi \frac{\partial S_a}{\partial t} + \nabla \cdot [\mathbf{F}(S_a, \mathbf{v}_t) - \lambda(S_a) \nabla p_c(S_a)] = 0, \\ &\nabla \cdot \mathbf{v}_t = 0, \end{aligned}\right\} \tag{8}$$

where

$$\begin{aligned} &\mathbf{F}(S_a, \mathbf{v}_t) = f_a(S_a) \mathbf{v}_t + \lambda(S_a)(\rho_w - \rho_a) g \mathbf{e}_z, \\ &\lambda(S_a) = \frac{\lambda_a(S_a) \lambda_w(1 - S_a)}{\lambda_a(S_a) + \lambda_w(1 - S_a)}. \end{aligned}$$

The vector-valued function $\mathbf{F}$ [m s^{-1}] and the scalar function λ [m^2 Pa^{-1} s^{-1}] are respectively referred to as the *flux* and *mobility* function. Define the *average fluid pressure* p by

$$p = \frac{p_a + p_w}{2},$$

then $p_a = p + p_c(S_a)/2$ and $p_w = p - p_c(S_a)/2$, thus from $\mathbf{v}_t = \mathbf{v}_a + \mathbf{v}_w$ and (4) we obtain

$$\begin{aligned} \mathbf{v}_t = -[&(\lambda_a(S_a) + \lambda_w(1 - S_a)) \nabla p + \frac{\lambda_a(S_a) - \lambda_w(1 - S_a)}{2} \nabla p_c(S_a) \\ &+ (\rho_a \lambda_a(S_a) + \rho_w \lambda_w(1 - S_a)) g \mathbf{e}_z]. \end{aligned} \tag{9}$$

The equations (8) and (9) result into the *fractional flow model*:

$$\left.\begin{aligned} &\phi \frac{\partial S_a}{\partial t} + \nabla \cdot [\mathbf{F}(S_a, \mathbf{v}_t) - \lambda(S_a) \nabla p_c(S_a)] = 0, \\ &\nabla \cdot [(\lambda_a(S_a) + \lambda_w(1 - S_a)) \nabla p + \frac{\lambda_a(S_a) - \lambda_w(1 - S_a)}{2} \nabla p_c(S_a)] \\ &\quad + g \frac{\partial}{\partial z} (\rho_a \lambda_a(S_a) + \rho_w \lambda_w(1 - S_a)) = 0. \end{aligned}\right\} \tag{10}$$

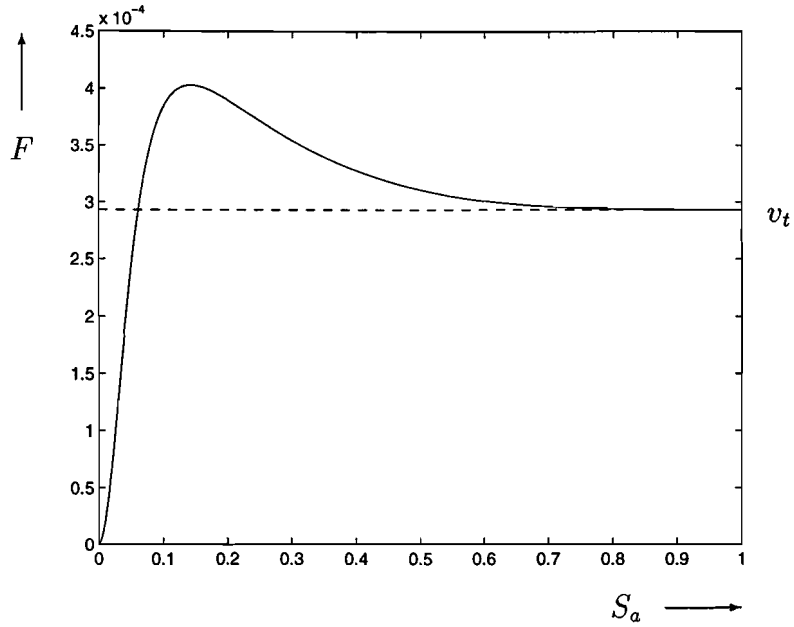

Figure 3: Typical flux function

These equations are respectively called the saturation and pressure equation. It is also possible to write the saturation equation as

$$\phi \frac{\partial S_a}{\partial t} + \nabla \cdot [\mathbf{F}(S_a, \mathbf{v}_t) - D(S_a)\nabla S_a] = 0, \tag{11}$$

where the *capillary diffusion* function D [m^2 s^{-1}] is defined by

$$D(S_a) = \lambda(S_a)p_c'(S_a). \tag{12}$$

The flux and capillary diffusion function are highly non-linear. The flux function represents convective transport of the air phase and includes gravitational effects. The capillary diffusion function represents diffusive transport caused by capillary suction. It is only defined for $0 < S_a < 1$. If the system becomes completely air-saturated, i.e. $S_a \uparrow 1$, then $\mathbf{F}(S_a, \mathbf{v}_t) \rightarrow \mathbf{v}_t$ and $D(S_a) \downarrow 0$. The relative air-permeability is now uniformly equal to 1, capillary forces no longer play a role and the flow described by (8) is entirely convection-driven, i.e. it reduces to *saturated* Darcy air flow. In this case the first equation of (8) is identical to (3) for $l = a$. In the opposite case where water saturation uniformly approaches one, i.e. $S_a \downarrow 0$, we have $\mathbf{F}(S_a, \mathbf{v}_t) \rightarrow \mathbf{0}$ and $D(S_a) \downarrow 0$. Equations (8) now degenerate as they only relate to the air phase. However, similar equations as (8) can be derived for the water phase. It is easily verified that these equations reduce to saturated water flow as described by (3) for $l = w$.
The above described behaviour is illustrated by Figures 3 and 4 in which graphs of $F_z(S_a, \mathbf{v}_t)$ and $D(S_a)$ are depicted for $K = 5.3 \cdot 10^{-11}$ m^2 and $v_{t,z} = 0.293$ mm s^{-1}. The values used for the other relevant parameters can be found listed at the end of this article.

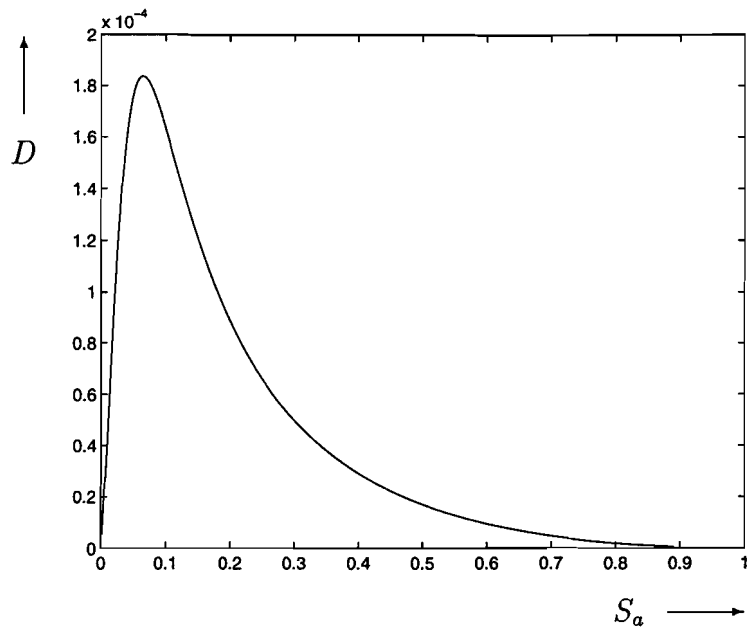

Figure 4: Typical diffusion function

Figure 3 also shows that F_z is not necessarily monotone in S_a. This is due to the presence of gravity in the system. The following theorem gives a condition for the monotonicity of F_z (see also [2]).

THEOREM: $F_z(\bullet, \mathbf{v}_t)$ is an increasing function if, and only if,

$$v_{t,z} \leq -\frac{K(\rho_w - \rho_a)g}{\mu_a} \text{ or } v_{t,z} \geq \frac{K(\rho_w - \rho_a)g}{\mu_w}. \tag{13}$$

Moreover, if $F_z(\bullet, \mathbf{v}_t)$ is not increasing, then the equation $F_z(S, \mathbf{v}_t) = v_{t,z}$ has exactly one solution $S \in (0,1)$. In this case $F_z(\bullet, \mathbf{v}_t)$ is increasing on $(0, S)$ if $v_{t,z} > 0$, and $v_{t,z} < 0$ implies that $F_z(\bullet, \mathbf{v}_t)$ is decreasing on $(S, 1)$.

PROOF: If $v_{t,z} = 0$, then $F_z(\bullet, \mathbf{v}_t)$ is not increasing. Thus assume $v_{t,z} \neq 0$ and denote

$$\kappa = \frac{(\rho_w - \rho_a)g}{v_{t,z}}.$$

Define $F(S) = f_a(S)[1 + \kappa\lambda_w(1-S)]$, $0 < S < 1$. Let $-\mu_w \leq \kappa K \leq \mu_a$, then $1 + \kappa\lambda_w(1 - S) > 0$ and $1 - \kappa\lambda_a(S) > 0$ for all $S \in (0,1)$, thus

$$F'(S) = \frac{\lambda_w(1-S)[1+\kappa\lambda_w(1-S)]\lambda_a'(S) + \lambda_a(S)[1-\kappa\lambda_a(S)]\lambda_w'(1-S)}{[\lambda_a(S) + \lambda_w(1-S)]^2} > 0,$$
$$0 < S < 1.$$

Let $\kappa K > \mu_a$, then there exists some $S \in (0,1)$ such that $\kappa\lambda_a(S) > 1$, i.e.

$$F(S) = \frac{\lambda_a(S) + \kappa\lambda_a(S)\lambda_w(1-S)}{\lambda_a(S) + \lambda_w(1-S)} > 1.$$

Since $\lim_{S\downarrow 0} F(S) = 0$ and $\lim_{S\uparrow 1} F(S) = 1$ it follows that F is not increasing. Furthermore,

$$\kappa\lambda_a(S) > 1 \Leftrightarrow F(S) > 1,$$
$$\kappa\lambda_a(S) < 1 \Leftrightarrow F(S) < 1.$$

Therefore the equation $F(S) = 1$ has exactly one solution $S \in (0,1)$, and F is increasing on $(0, S)$.
Let $\kappa K < -\mu_w$, then there exists some $S \in (0,1)$ such that $\kappa\lambda_w(1-S) < -1$, i.e. $F(S) < 0$, which implies that F is not increasing. Furthermore,

$$\kappa\lambda_w(1-S) < -1 \Leftrightarrow F(S) < 0,$$
$$\kappa\lambda_w(1-S) > -1 \Leftrightarrow F(S) > 0.$$

Therefore the equation $F(S) = 1$ has exactly one solution $S \in (0,1)$, and F is increasing on $(S, 1)$. □

Equation (13) balances some vertical Darcy velocity due to gravitational pull and the vertical component of the total Darcy velocity $\mathbf{v}_t$, which also incorporates capillary diffusion.
In Figure 3 condition (13) does not hold for $v_{t,z} = 0.293$ mm s^{-1}. It appears that $F_z(S_a) = v_{t,z}$ for $S_a \approx 0.061$. This corresponds to a steady-state solution for problem (8). Apparently, (13) provides the maximum allowable magnitude $v_{t,z} \approx 29.3$ mm s^{-1} for the vertical component of the Darcy velocity in order that a uniform steady-state solution is available. For larger values of $v_{t,z}$ capillary action causes the steady state solution to be non-uniform.
When comparing Figures 3 and 4, first it appears that $F_z(S_a, \mathbf{v}_t)$ is generally larger than $D(S_a)|\nabla S_a|$ as long as $|\nabla S_a|$ is smaller than 1.6 m^{-1}. Second, as S_a approaches one the contribution of D dies out rapidly. Our system seems to be dominated by convection. At this point it is stressed that the first expression of (8) changes from a *parabolic* into a *hyperbolic* partial differential equation with the disappearance of the diffusion function. This observation will eventually enable us to identify appropriate numerical techniques.
If $\mathbf{v}_t$ is chosen such that $\nabla \cdot \mathbf{v}_t = 0$, then the remaining equation of (8) is a non-linear convection-diffusion equation in terms of S_a only. Choosing $\mathbf{v}_t$ this way is a common approach to understand the qualitative behaviour of the solution. We shall use this approach in our study of the one-dimensional case in the next section.

3 One-dimensional modelling

In this section the simple one-dimensional instationary case is studied in order to gain insight in the various physical and numerical problems encountered in modelling the air sparging process. First, a mathematical statement of the one-dimensional problem is given using the fractional flow approach discussed at the end of the previous section. The mass

conservation equation is classified for as much as its non-linear nature allows. The Godunov scheme and a high resolution scheme are outlined and tested.

3.1 One-dimensional fractional flow model

3.1.1 Governing equations

We will consider *vertical* upward flow resulting from a constant vertical injection of air at a certain depth. Thus, consider the one-dimensional fractional flow model for air saturation resulting from (8):

$$\phi\frac{\partial S}{\partial t}+\frac{\partial}{\partial z}\left(F(S)-\lambda(S)\frac{\partial}{\partial z}p_c(S)\right)=0, \tag{14}$$

$$\frac{\partial v_t}{\partial z}=0, \tag{15}$$

where $F(S)=f_a(S)v_t+\lambda(S)(\rho_w-\rho_a)g$. From (15) it is clear that v_t is uniform.
Suppose that (14) holds for $-h_b<z<h_t$. The lower boundary $z=-h_b$ is located at the position of the vertical air injection, i.e. the boundary condition at $z=-h_b$ is

$$F(S)-\lambda(S)\frac{\partial}{\partial z}p_c(S)=v_{in}. \tag{16}$$

From this it follows that $v_t=v_{in}$ and thus

$$F(S)=f_a(S)v_{in}+\lambda(S)(\rho_w-\rho_a)g.$$

We locate the upper boundary sufficiently high above the natural water table at $z=0$. At the upper boundary $z=h_t$ we impose the natural outflow condition

$$\frac{\partial S}{\partial z}=0. \tag{17}$$

As an alternative the condition $S=1$ can be used. Both conditions mimic the infinite boundary condition $\lim_{z\to\infty}S(z)=1$. We assume the natural no-flow equilibrium as initial condition. Thus, initially the water table is located at $z=0$, i.e. $S(z)=0$ if $z\leq 0$. The no-flow saturation distribution above the water table now follows as the solution of the one-dimensional analogon of (4). Thus, $p_w=-\rho_w gz$ and $p_a=-\rho_a gz$ for $z\geq 0$, and from the first equation of (5) it follows that

$$\frac{(\rho_w-\rho_a)g}{\alpha}\left((1-S(z))^{-1/m}-1\right)^{1-m}=p_c(S(z))=(\rho_w-\rho_a)gz.$$

Therefore,

$$S(z)=1-\left((\alpha z)^{\frac{1}{1-m}}+1\right)^{-m},\ z\geq 0$$

(see Figure 5). Indeed, $S(0)=0$ and $\lim_{z\to\infty}S(z)=1$.

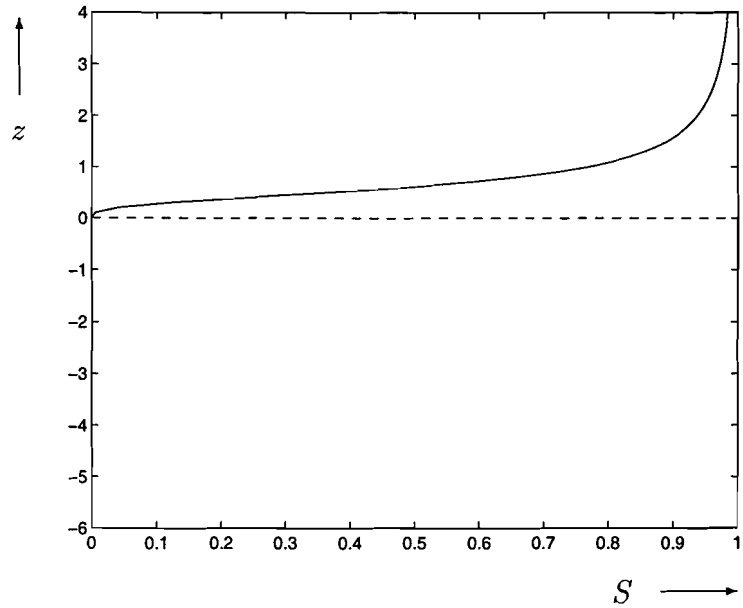

Figure 5: Initial saturation distribution

3.1.2 The hyperbolic problem

Since (14) is assumed to be dominated by convection, we will consider the hyperbolic conservation law

$$\phi \frac{\partial S}{\partial t} + \frac{\partial}{\partial z} F(S) = 0 \tag{18}$$

with the boundary condition $F(S) = v_{in}$ at $z = -h_b$ and the initial condition $S(z) = 0$, $z > -h_b$, i.e. we do not consider the unsaturated zone.
First consider the case that F is not increasing. Let S_0 be the solution of the equation $F(S) = v_{in}$, and F_c be the concave envelope of F (see Figure 6). We assume that for some $S_c \in (0, S_0)$,

$$F_c(S) = \begin{cases} F(S_c)S/S_c, & 0 \le S \le S_c, \\ F(S), & S_c \le S \le S_0. \end{cases}$$

Let $v_c = F'(S_c)/\phi$ and $v_0 = F'(S_0)/\phi$, then the solution of (18) is (see Figure 7)

$$S(x,t) = \begin{cases} S_0, & 0 \le z + h_b \le v_0 t, \\ \bar{S} \text{ such that } (z+h_b)\phi = F'(\bar{S})t, & v_0 t \le z + h_b < v_c t, \\ 0, & z + h_b > v_c t. \end{cases}$$

In the case that F is increasing we obtain the same solution except that $S_0 = 1$. For a detailed derivation see [4].

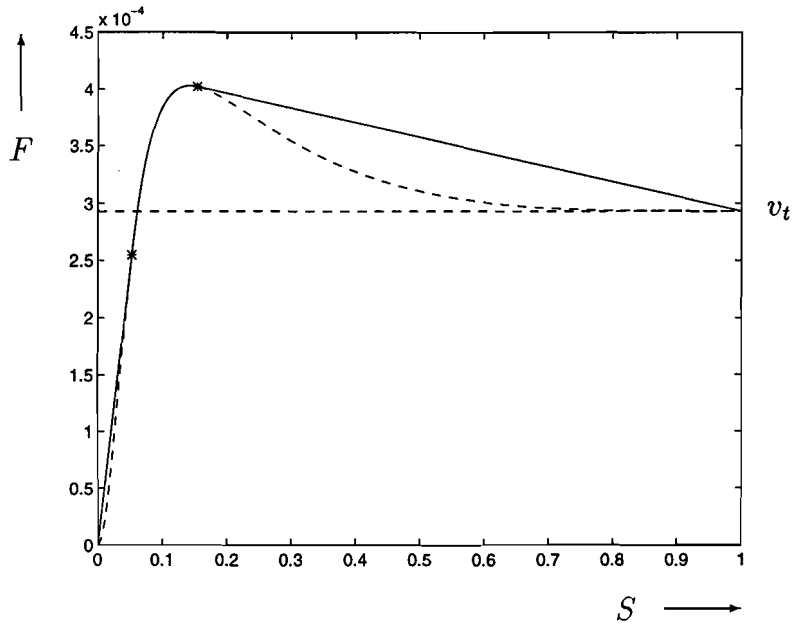

Figure 6: Concave envelope of the flux function

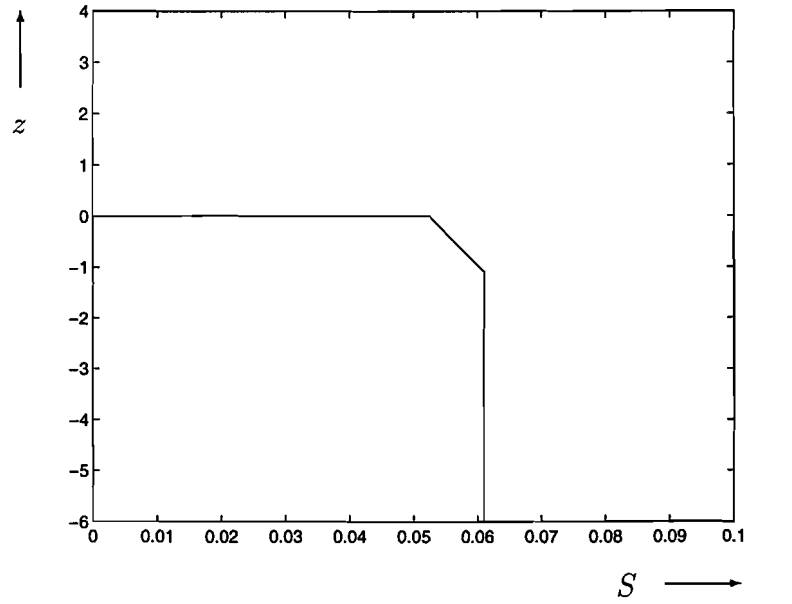

Figure 7: Solution of the hyperbolic problem at $t = h_b/v_c$

3.2 Numerical methods

Based on the previous sections, we know that the differential equation (14) is a non-linear parabolic equation. As the contribution of diffusion is expected to be small, however, we may classify our equation equally well as *quasi*-hyperbolic. Characteristic of solutions of hyperbolic conservation laws is that initially discontinous data may cause the solution to remain discontinuous while propagating. Solutions of parabolic laws, to the contrary, will always be smooth regardless of the initial data.
Prior to the implementation of the air sparging model it makes sense to have this discussion as, from a physical point of view, we do not yet know how 'sharp' the air-saturated front will be immediately after switching on the injection system. That is the reason why (14) is regarded as both a parabolic and a quasi-hyperbolic equation in order that suitable numerical methods can be proposed.
To discretise (14) the domain $[-h_b, h_t]$ is divided into M cells of equal width Δz. This gives M nodes $z_j = -h_b + (j - 1/2)\Delta z$, $j = 1, \ldots, M$, where $\Delta z = (h_b + h_t)/M$. The nodes z_j are the centres of the grid cells. The boundaries of the computational domain coincide with the outer edges of the outer cells. Using this *block-centred* approach, the air saturation S is approximated at the cell centres, giving unique values per cell. After collecting those values, a piecewise continuous approximation for the saturation profile is constructed. The Darcy velocities are approximated at the interfaces $z_{j+1/2}$ between the cells, thus allowing mass conservation to be easily monitored and secured per cell.
Time-sampling takes place at $t_n = n\Delta t, n = 0, 1, \ldots$, where Δt is the time step. We write S_j^n for a numerical approximation of the exact solution $S(z_j, t_n)$. The governing equation is represented by $M - 2$ difference equivalents, discretised at time levels t_n and t_{n+1}, and at nodes z_j with $j = 2, \ldots, M - 1$. The boundary conditions at $z = -h_b$ and $z = h_t$ provide the remaining equations necessary to solve the system.

3.2.1 The Godunov scheme

The first scheme considered is the Godunov scheme (see [7], [8] and [4]). It is used in a modified version because of the presence of a diffusive term. The scheme is explicit, i.e. all values for S calculated at the new time level are functions of values at the previous time level only. With respect to computational effort, this is a very attractive feature of this scheme. On the other hand, however, the time step is limited by the *Courant-Friedrichs-Lewy* condition $CFL \leq 1$, where

$$CFL = \frac{\Delta t}{\phi \Delta z} \max_{0 \leq S \leq 1} |F'(S)|$$

is the Courant number. The Godunov scheme for hyperbolic conservation laws is based on solving *Riemann problems* at the interfaces $z_{j+1/2}$ between grid cells. At each time level the numerical solution of the previous time level serves as initial data. The solutions of the Riemann problems are assembled to form a piecewise *constant* numerical solution at the new time level.

Consider for the time being the hyperbolic problem (18). Provided that $CFL \leq 1$, the Godunov scheme is

$$S_j^{n+1} = S_j^n - \frac{\Delta t}{\phi \Delta z}[F(S_{\mathcal{R}}(0; S_j^n, S_{j+1}^n)) - F(S_{\mathcal{R}}(0; S_{j-1}^n, S_j^n))]. \tag{19}$$

The function $S_{\mathcal{R}}(\bullet; S_j^n, S_{j+1}^n)$ is defined by

$$S_{\mathcal{R}}\left(\frac{z - z_{j+1/2}}{t - t_n}; S_j^n, S_{j+1}^n\right) = W(z,t),$$

where W is the solution of the Riemann problem for the interface $z_{j+1/2}$, i.e.

$$\phi \frac{\partial W}{\partial t} + \frac{\partial}{\partial z} F(W) = 0,$$
$$W(z, t_n) = \begin{cases} S_j^n, & z < z_{j+1/2}, \\ S_{j+1}^n, & z > z_{j+1/2}. \end{cases}$$

Equation (19) results from averaging the juxtaposition $S_{\mathcal{R}}^{n+1}$ of the Riemann solutions $S_{\mathcal{R}}(\bullet; S_j^n, S_{j+1}^n)$ over the corresponding grid cells at time level t_{n+1}, i.e.

$$S_j^{n+1} = \frac{1}{\Delta z} \int_{z_{j-1/2}}^{z_{j+1/2}} S_{\mathcal{R}}^{n+1}(z)\, dz.$$

It can be shown (see [8]) that

$$F(S_{\mathcal{R}}(0; S_j^n, S_{j+1}^n)) = \begin{cases} \min\limits_{S_j^n \leq S \leq S_{j+1}^n} F(S) \text{ if } S_j^n \leq S_{j+1}^n, \\ \max\limits_{S_{j+1}^n \leq S \leq S_j^n} F(S) \text{ if } S_j^n \geq S_{j+1}^n. \end{cases}$$

If (13) holds, then F is an increasing function and thus $F(S_{\mathcal{R}}(0; S_j^n, S_{j+1}^n)) = F(S_j^n)$. If (13) does not hold, then the computation of $F(S_{\mathcal{R}}(0; S_j^n, S_{j+1}^n))$ is more complicated. We assume, however, that in this case F has exactly one stationary point, i.e. the equation $F'(S) = 0$ has a unique solution $S \in (0,1)$. As a result from this assumption, F is increasing on $(0, S)$ and decreasing on $(S, 1)$.
The Godunov scheme is monotone (see [8] and [4]) and therefore it is only first order accurate. Note that a monotone scheme is total variation diminishing (TVD), i.e. $TV(S^{n+1}) \leq TV(S^n)$, where

$$TV(S) = \sum_{j=1}^{N-1} |S_{j+1} - S_j|.$$

With the definition $S_{j+1/2}^n = (S_j^n + S_{j+1}^n)/2$, a possible modification of the Godunov scheme for problem (14) results into the explicit scheme

$$S_j^{n+1} = S_j^n - \frac{\Delta t}{\phi \Delta z}[f_G(S_j^n, S_{j+1}^n) - f_G(S_{j-1}^n, S_j^n)], \tag{20}$$

where

$$f_G(S_j, S_{j+1}) = F(S_{\mathcal{R}}(0; S_j, S_{j+1})) - \lambda(S_{j+1/2}) \frac{p_c(S_{j+1}) - p_c(S_j)}{\Delta z}.$$

The construction of S_1^{n+1} and S_M^{n+1} has to be chosen differently in order to incorporate the boundary conditions. The inflow boundary condition (16) leads to

$$S_1^{n+1} = S_1^n - \frac{\Delta t}{\phi \Delta z}[f_G(S_1^n, S_2^n) - v_{in}],$$

and the natural outflow condition (17) results into

$$S_M^{n+1} = S_M^n - \frac{\Delta t}{\phi \Delta z}[F(S_M^n) - f_G(S_{M-1}^n, S_M^n)].$$

Since problem (14) is quasi-hyperbolic, i.e. dominated by convection, we limit the time step by $CFL \leq 1$. Even then the scheme (20) is not necessarily monotone. Since $\lim_{S \downarrow 0} D(S) = \lim_{S \uparrow 1} D(S) = 0$, it is impossible to give an upper bound for the quotient $\Delta t/(\Delta z)^2$ that guarantees monotonicity. A modification of the Godunov scheme that guarantees monotonicity is

$$\begin{aligned} S_j^{n+1} - \frac{\Delta t}{\phi \Delta z} \left[\lambda(S_{j+1/2}^{n+1}) \frac{p_c(S_{j+1}^{n+1}) - p_c(S_j^{n+1})}{\Delta z} - \lambda(S_{j-1/2}^{n+1}) \frac{p_c(S_j^{n+1}) - p_c(S_{j-1}^{n+1})}{\Delta z} \right] \\ = S_j^n - \frac{\Delta t}{\phi \Delta z} \left[F(S_{\mathcal{R}}(0; S_j^n, S_{j+1}^n)) - F(S_{\mathcal{R}}(0; S_{j-1}^n, S_j^n)) \right]. \end{aligned} \tag{21}$$

Incorporation of the boundary conditions into (21) results into a non-linear algebraic system of equations. Therefore we linearise this scheme resulting into

$$\left.\begin{aligned} S_j^{n+1/2} &= S_j^n - \frac{\Delta t}{\phi \Delta z} \left[F(S_{\mathcal{R}}(0; S_j^n, S_{j+1}^n)) - F(S_{\mathcal{R}}(0; S_{j-1}^n, S_j^n)) \right], \\ S_j^{n+1} - \frac{\Delta t}{\phi (\Delta z)^2} &\left[D(S_{j+1/2}^{n+1/2})(S_{j+1}^{n+1} - S_j^{n+1}) - D(S_{j-1/2}^{n+1/2})(S_j^{n+1} - S_{j-1}^{n+1}) \right] = 0. \end{aligned}\right\} \tag{22}$$

The inflow boundary condition (16) leads to

$$\left.\begin{aligned} S_1^{n+1/2} &= S_1^n - \frac{\Delta t}{\phi \Delta z} \left[F(S_{\mathcal{R}}(0; S_1^n, S_2^n)) - v_{in} \right], \\ S_1^{n+1} - \frac{\Delta t}{\phi (\Delta z)^2} &\left[D(S_{3/2}^{n+1/2})(S_2^{n+1} - S_1^{n+1}) \right] = 0. \end{aligned}\right\} \tag{23}$$

and the natural outflow condition (17) results into

$$\left.\begin{aligned} S_M^{n+1/2} &= S_M^n - \frac{\Delta t}{\phi \Delta z} \left[F(S_M^n) - F(S_{\mathcal{R}}(0; S_{M-1}^n, S_M^n)) \right], \\ S_M^{n+1} - \frac{\Delta t}{\phi (\Delta z)^2} &\left[D(S_M^{n+1/2})(1 - S_M^{n+1}) - D(S_{M-1/2}^{n+1/2})(S_M^{n+1} - S_{M-1}^{n+1}) \right] = 0. \end{aligned}\right\} \tag{24}$$

In the second equation of (24) we have used the boundary condition $S = 1$. The equations (22)–(24) are a linear system of equations with a tridiagonal coefficient matrix. Note that the scheme is conservative, i.e. it conserves mass and thus also volume.

3.2.2 A high resolution scheme

As an improvement of the first order accurate Godunov scheme, we consider a conservative scheme that is second order accurate in space. However, it is still first order accurate in time. So, the complete scheme is first order accurate with a possibly better resolution in space. Again, the scheme is based on solving Riemann problems at the interfaces $z_{j+1/2}$ between grid cells. At each time level the numerical solution of the previous time level serves as initial data. The solutions of the Riemann problems are assembled to form a piecewise *linear* numerical solution at the new time level. In order to prevent excessive oscillations, the slopes of this piecewise linear solution are limited by a *slope limiter*. If the time step is limited by $CFL \leq 1/2$, then the scheme is total variation diminishing. For details on this scheme, see [4], [7] and [8].
With the definition $S^n_{j+1/2} = (S^n_j + S^n_{j+1})/2$, the modification of the high resolution scheme for problem (14) results into the scheme

$$S^{n+1/2}_j = S^n_j - \frac{\Delta t}{\phi \Delta z}\left[F(S_{\mathcal{R}}(0; S^{n,-}_{j+1/2}, S^{n,+}_{j+1/2})) - F(S_{\mathcal{R}}(0; S^{n,-}_{j-1/2}, S^{n,+}_{j-1/2}))\right],$$
$$S^{n+1}_j - \frac{\Delta t}{\phi(\Delta z)^2}\left[D(S^{n+1/2}_{j+1/2})(S^{n+1}_{j+1} - S^{n+1}_j) - D(S^{n+1/2}_{j-1/2})(S^{n+1}_j - S^{n+1}_{j-1})\right] = 0.$$

The left and right values at the interfaces $z_{j+1/2}$ between grid cells are defined by

$$S^-_{j+1/2} = S_j + \sigma_j/2, \; S^+_{j+1/2} = S_{j+1} - \sigma_{j+1}/2,$$

where $\sigma_j = \text{minmod}(S_{j+1} - S_j, S_j - S_{j-1})$. The minmod function is defined by

$$\text{minmod}(a,b) = \begin{cases} a \text{ if } |a| < |b| \text{ and } ab > 0, \\ b \text{ if } |a| > |b| \text{ and } ab > 0, \\ 0 \text{ if } ab \leq 0. \end{cases}$$

Near the boundaries we define $\sigma_1 = \sigma_M = 0$. The construction of S^{n+1}_1 and S^{n+1}_M has to be chosen differently in order to incorporate boundary conditions. The inflow boundary condition (16) leads to

$$S^{n+1/2}_1 = S^n_1 - \frac{\Delta t}{\phi \Delta z}\left[F(S_{\mathcal{R}}(0; S^{n,-}_{3/2}, S^{n,+}_{3/2})) - v_{in}\right],$$
$$S^{n+1}_1 - \frac{\Delta t}{\phi(\Delta z)^2}\left[D(S^{n+1/2}_{3/2})(S^{n+1}_2 - S^{n+1}_1)\right] = 0.$$

and the natural outflow condition (17) results into

$$S^{n+1/2}_M = S^n_M - \frac{\Delta t}{\phi \Delta z}\left[F(S^n_M) - F(S_{\mathcal{R}}(0; S^{n,-}_{M-1/2}, S^{n,+}_{M-1/2}))\right],$$
$$S^{n+1}_M - \frac{\Delta t}{\phi(\Delta z)^2}\left[D(S^{n+1/2}_M)(1 - S^{n+1}_M) - D(S^{n+1/2}_{M-1/2})(S^{n+1}_M - S^{n+1}_{M-1})\right] = 0.$$

M	$N = \frac{4}{5}M$	$N = \frac{8}{5}M$
20	$2.2012 \cdot 10^{-3}$	$4.3632 \cdot 10^{-3}$
40	$1.4059 \cdot 10^{-3}$	$2.7917 \cdot 10^{-3}$
80	$8.7845 \cdot 10^{-4}$	$1.7572 \cdot 10^{-3}$
160	$5.4084 \cdot 10^{-4}$	$1.0909 \cdot 10^{-3}$

Table 1: Discretisation errors for the Godunov scheme

M	$N = \frac{8}{5}M$
20	$1.5209 \cdot 10^{-3}$
40	$7.1967 \cdot 10^{-4}$
80	$3.0990 \cdot 10^{-4}$
160	$1.6375 \cdot 10^{-4}$

Table 2: Discretisation errors for the high resolution scheme

3.2.3 Numerical experiments

As there is no analytic solution available for (14), we cannot assess the reliability of the numerically generated solutions directly.
Therefore, we first consider the hyperbolic problem (18) with the boundary condition $F(S) = v_{in}$ at $z = -h_b$ and the initial condition $S(z) = 0, z > -h_b$. Let $h_t = 4$ m, $h_b = 6$ m, $v_{in} = 0.293$ mm s^{-1} and the other relevant parameters be chosen as listed at the end of this article, then $S_0 \approx 0.0610$ and $S_c \approx 0.0525$. Thus $v_0 \approx 10.2$ mm s^{-1} and $v_c \approx 12.5$ mm s^{-1}. We consider the solution at time $t = h_b/v_c \approx 481.3$ s (see Figure 7).
The domain $[-h_b, h_t]$ is divided into M cells of equal width Δz. Time-sampling takes place at $t_n = n\Delta t$, $n = 0, 1, \ldots, N$, where $\Delta t = t/N$ is the time step. Limiting the time step by $CFL \leq 1$ results into the condition $\Delta t \lesssim 62.25\,\Delta z$. This condition is fulfilled by choosing, e.g., $M = 20$ and $N = 16$. In Tables 1 and 2 the discretisation error $\frac{1}{M}\sum_{j=1}^{M} |S_j^N - S(x_j, t)|$ is displayed for the Godunov scheme and the high resolution scheme.
From Table 1 it appears that the Godunov scheme is first order accurate. Given some cell width Δz, choosing Δt smaller than the maximal value resulting from $CFL \leq 1$ does not result into a more accurate solution.
The high resolution scheme generates a more accurate solution than the Godunov scheme. For a fair comparison of Table 1 and 2 one should realise that the computational work is linearly proportional to M and N. The high resolution scheme is also first order accurate.
As a second numerical experiment (14) is solved for $v_{in} = 0.293$ mm s^{-1}. Again the solution at time $t = h_b/v_c$ is considered. The results for the Godunov scheme and the high resolution scheme are displayed in Figures 8 and 9. The high resolution scheme gives slightly better results, but needs more computations.

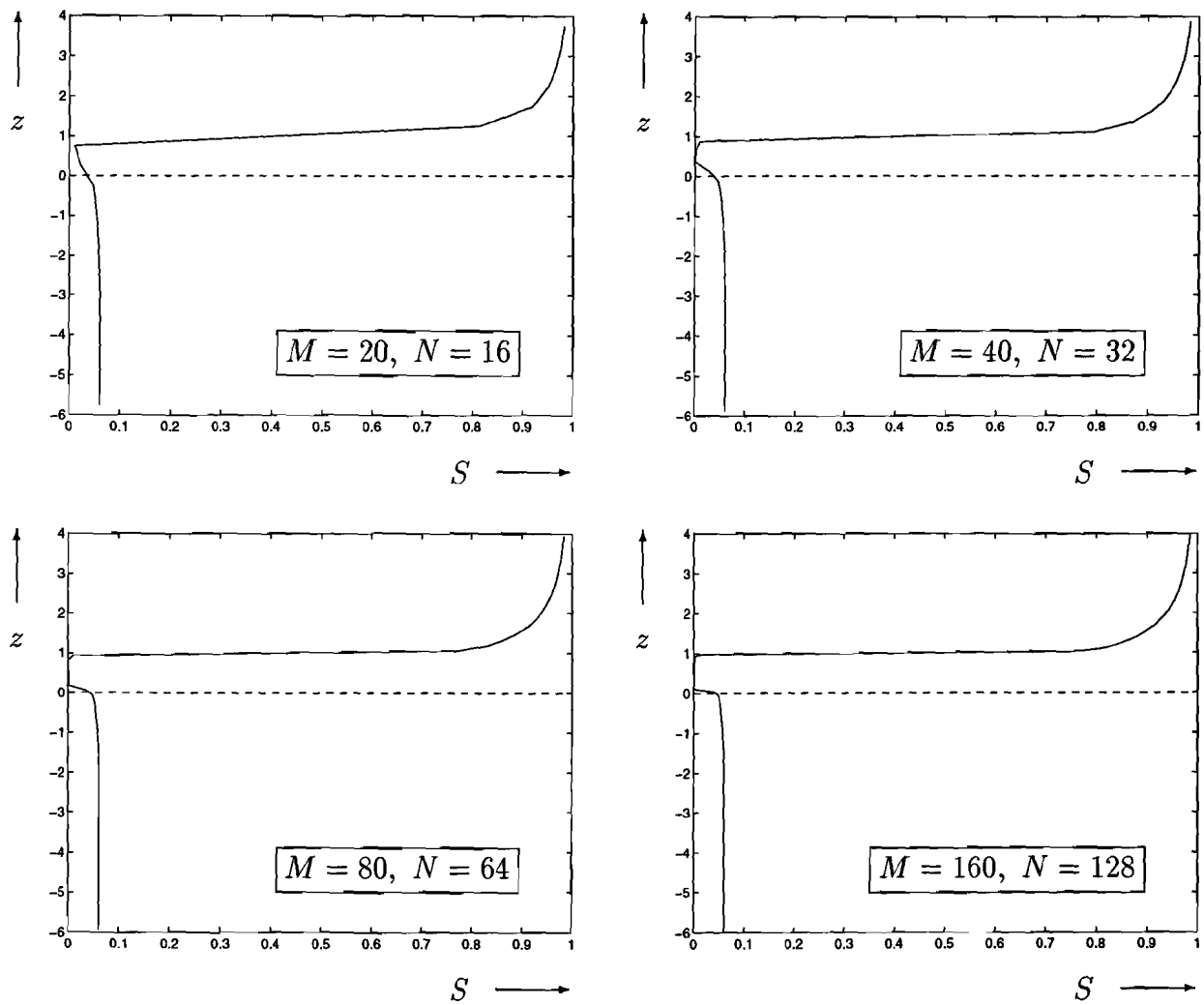

Figure 8: Solution for the Godunov scheme

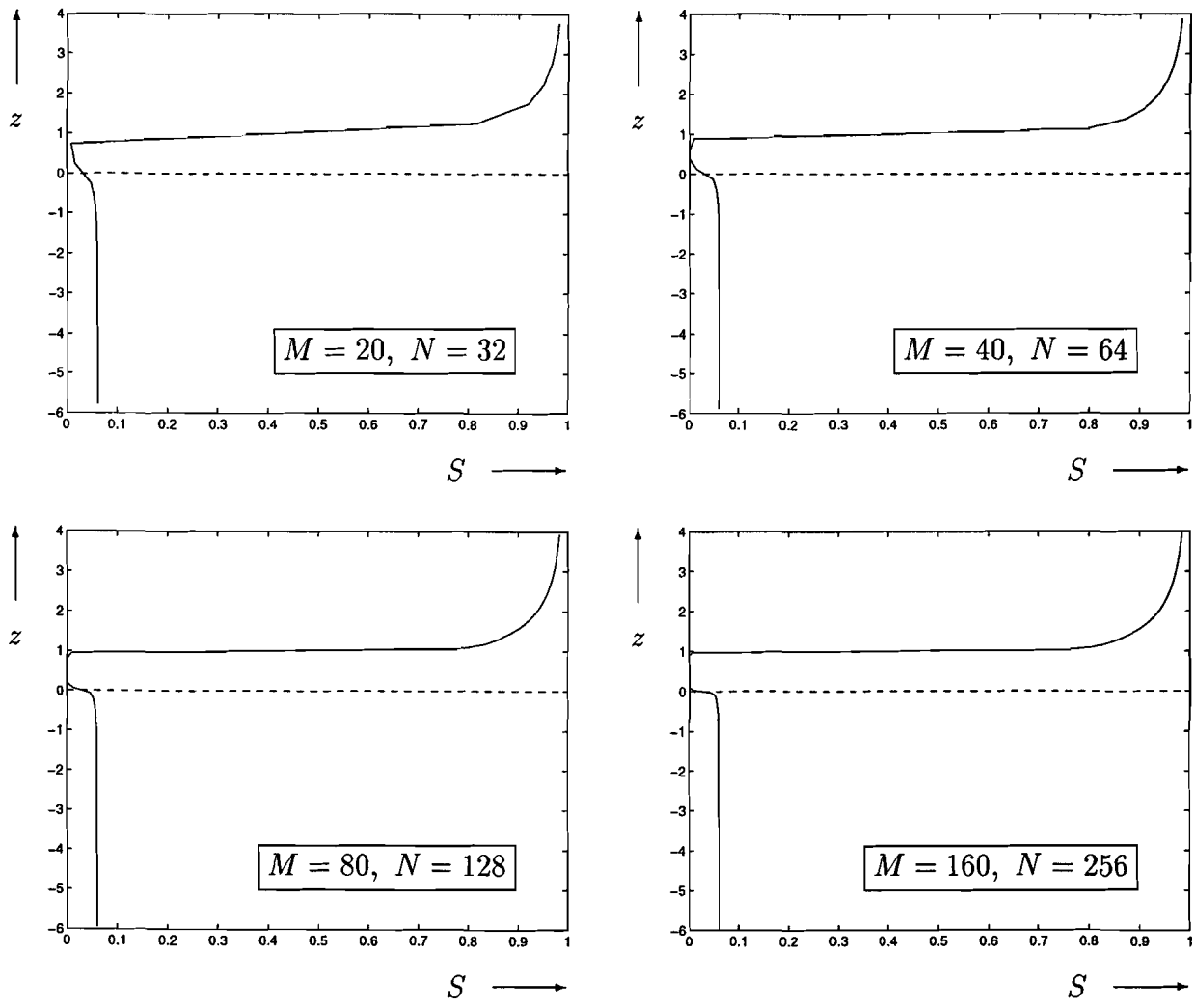

Figure 9: Solution for the high resolution scheme

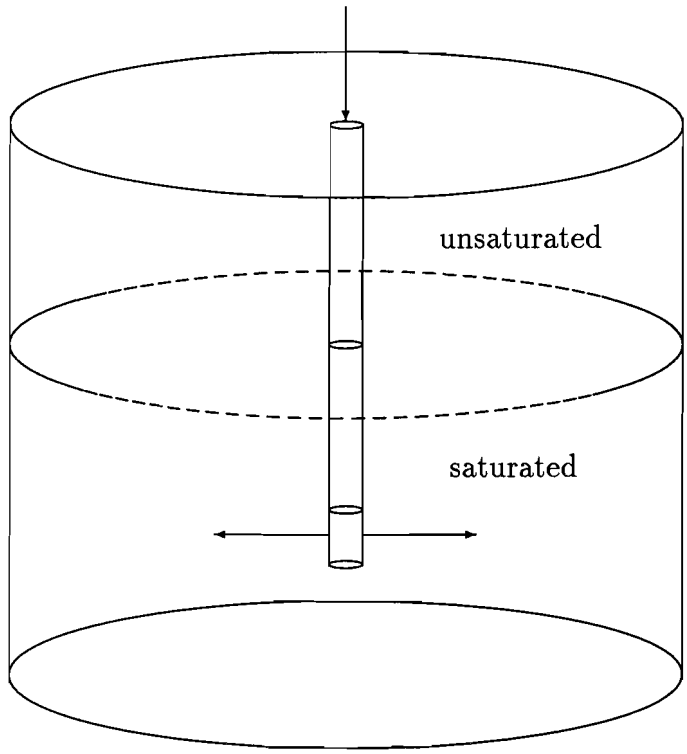

Figure 10: Physical domain

It can be observed that the water table is forced upwards due to the assumption of incompressibility of both phases. This is, however, a relatively slow process as the water phase must penetrate the unsaturated zone where initial permeability is low due to large air saturations.

4 Multi-dimensional modelling

4.1 Governing equations

Consider the three-dimensional fractional flow model (10), combining the saturation and pressure equation. The total Darcy velocity $\mathbf{v}_t$ is given by (9). As in Section 3, we will denote the air saturation by S. If S is assumed to be known, then the pressure equation is a linear elliptic equation for the average fluid pressure p.
We will consider axially symmetric flow resulting from a constant injection of air through an injection filter (see Figure 10). In order to describe this situation properly, we introduce

exponential cylindrical coordinates r, θ and z, i.e.

$$\mathbf{x} = \begin{pmatrix} e^r \cos\theta \\ e^r \sin\theta \\ z \end{pmatrix}.$$

The choice of these coordinates implies a refinement of the numerical grid near the injection filter (see Section 4.2). If the boundary conditions and initial conditions are chosen such that the solution does not depend on θ, then the fractional flow model (10) can be rewritten as

$$\begin{aligned} &\phi\frac{\partial S}{\partial t} + e^{-2r}\frac{\partial}{\partial r}\left[e^r F_r(S, v_t) - \lambda(S)\frac{\partial}{\partial r}p_c(S)\right] \\ &\quad + \frac{\partial}{\partial z}\left[F_z(S, v_t) - \lambda(S)\frac{\partial}{\partial z}p_c(S)\right] = 0, \end{aligned} \tag{25}$$

$$\begin{aligned} &e^{-2r}\frac{\partial}{\partial r}\left[(\lambda_a(S) + \lambda_w(1-S))\frac{\partial p}{\partial r} + \frac{\lambda_a(S) - \lambda_w(1-S)}{2}\frac{\partial}{\partial r}p_c(S)\right] \\ &\quad + \frac{\partial}{\partial z}\left[(\lambda_a(S) + \lambda_w(1-S))\frac{\partial p}{\partial z} + \frac{\lambda_a(S) - \lambda_w(1-S)}{2}\frac{\partial}{\partial z}p_c(S)\right] \\ &\quad + g\frac{\partial}{\partial z}(\rho_a\lambda_a(S) + \rho_w\lambda_w(1-S)) = 0, \end{aligned} \tag{26}$$

where the horizontal and vertical components of the flux function are given by

$$\begin{aligned} F_r(S, v_{t,r}) &= f_a(S)v_{t,r}, \\ F_z(S, v_{t,z}) &= f_a(S)v_{t,z} + \lambda(S)(\rho_w - \rho_a)g. \end{aligned}$$

Suppose that these equations hold for $-h_b < z < h_t$ and $r_{in} < r < r_{out}$, i.e. the bottom of the physical domain is located at $z = -h_b$ and the top at $z = h_t$, and the radius of the filter and the physical domain are respectively equal to $e^{r_{in}}$ and $e^{r_{out}}$. Air is injected through the filter, i.e. the boundary conditions at $-h_l < z < -h_u$ and $r = r_{in}$ are

$$F_r(S, v_{t,r}) - \lambda(S)e^{-r}\frac{\partial}{\partial r}p_c(S) = v_{in}, \tag{27}$$

$$v_{t,r} = v_{in}. \tag{28}$$

The top boundary $z = h_t$ is located sufficiently high above the natural water table at $z = 0$. At this boundary we impose the natural outflow condition

$$\frac{\partial S}{\partial z} = 0, \tag{29}$$

combined with the condition $S = 1$. We assume the pressure corresponding to the natural no-flow equilibrium as the other boundary condition, i.e.

$$p = -\frac{\rho_a + \rho_w}{2}gh_t. \tag{30}$$

At the remainder of the inner boundary $r = r_{in}$ the no-flow boundary condition is imposed. At the bottom boundary $z = -h_b$ an impermeable bedrock is assumed. Suppose that $r_{out} \gg r_{in}$, then at the outer boundary $r = r_{out}$ the influence of the air injection can be neglected. Therefore, the no-flow boundary condition is also supposed to hold at this boundary, i.e.

$$F_r(S, v_{t,r}) - \lambda(S)e^{-r}\frac{\partial}{\partial r}p_c(S) = 0, \tag{31}$$

$$v_{t,r} = 0. \tag{32}$$

We assume the natural no-flow equilibrium as initial condition (see Section 3.1.1). Note that there is no need for an initial condition for the total pressure p.

4.2 Numerical methods

In the one-dimensional case it is a trivial matter to compute the total Darcy velocity v_t. The solution, i.e. $v_t = v_{in}$, can be used in the flux function F to compute the air saturation S. Computing $\mathbf{v}_t$ in the multi-dimensional case is certainly not as obvious. At each time level (26) has to be solved numerically for some approximate saturation S.
The interval $[r_{in}, r_{out}]$ is divided into M_r cells of equal width Δr. Note that this choice generates a refinement of the numerical grid near the injection filter. The interval $[-h_b, h_t]$ is divided into M_z cells of equal width Δz. Thus, the computational domain $[r_{in}, r_{out}] \times [-h_b, h_t]$ is divided into $M_r M_z$ cells with centres (r_i, z_j), where $r_i = r_{in} + (i - 1/2)\Delta r$, $i = 1, \ldots, M_r$, and $z_j = -h_b + (j - 1/2)\Delta z$, $j = 1, \ldots, M_z$. The air saturation S and pressure p are approximated at the cell centres, giving unique values per cell. The Darcy velocity $\mathbf{v}_t$ is approximated at the interfaces between the cells.
Time-sampling takes place at $t_n = n\Delta t$, $n = 0, 1, \ldots$, where Δt is the time step. We write S_{ij}^n and p_{ij}^n for the numerical approximations of the exact solutions $S(r_i, z_j, t_n)$ and $p(r_i, z_j, t_n)$. The governing equations are represented by $(M_r - 2)(M_z - 2)$ difference equivalents, discretised at time levels t_n and t_{n+1}, and at nodes (r_i, z_j), where $i = 2, \ldots, M_r - 1$, and $j = 2, \ldots, M_z - 1$. The boundary conditions provide the remaining equations necessary to solve the systems.

4.2.1 The Godunov scheme for the saturation equation

We consider the multi-dimensional version of the Godunov scheme (see [5]). With the definitions $S_{i+1/2,j}^n = (S_{i+1,j}^n + S_{ij}^n)/2$ and $S_{i,j+1/2}^n = (S_{i,j+1}^n + S_{ij}^n)/2$, the modification of

this scheme for problem (25) results into the scheme

$$\left.\begin{aligned}
&S_{ij}^{n+1/2} = S_{ij}^n - \frac{\Delta t}{\phi \Delta R_i^2}\Big[R_{i+1/2}F_r(S_{\mathcal{R}}(0; S_{ij}^n, S_{i+1,j}^n), v_{i+1/2,j}^n) \\
&\quad - R_{i-1/2}F_r(S_{\mathcal{R}}(0; S_{i-1,j}^n, S_{ij}^n), v_{i-1/2,j}^n)\Big] \\
&\quad - \frac{\Delta t}{\phi \Delta z}\Big[F_z(S_{\mathcal{R}}(0; S_{ij}^n, S_{i,j+1}^n), v_{i,j+1/2}^n) - F_z(S_{\mathcal{R}}(0; S_{i,j-1}^n, S_{ij}^n), v_{i,j-1/2}^n)\Big], \\
&\Delta z \Delta R_i^2 S_{ij}^{n+1} - \frac{\Delta t \Delta z}{\phi}\left[\frac{R_{i+1/2}}{\Delta R_{i+1/2}} D(S_{i+1/2,j}^{n+1/2})(S_{i+1,j}^{n+1} - S_{ij}^{n+1})\right. \\
&\quad \left. - \frac{R_{i-1/2}}{\Delta R_{i-1/2}} D(S_{i-1/2,j}^{n+1/2})(S_{ij}^{n+1} - S_{i-1,j}^{n+1})\right] \\
&\quad - \frac{\Delta t \Delta R_i^2}{\phi \Delta z}\Big[D(S_{i,j+1/2}^{n+1/2})(S_{i,j+1}^{n+1} - S_{ij}^{n+1}) - D(S_{i,j-1/2}^{n+1/2})(S_{ij}^{n+1} - S_{i,j-1}^{n+1})\Big] = 0.
\end{aligned}\right\} \quad (33)$$

For notational convenience we denote $R_{i+1/2} = e^{r_{i+1/2}}$, $\Delta R_{i+1/2} = e^{r_{i+1}} - e^{r_i}$ and $\Delta R_i^2 = e^{2r_{i+1/2}} - e^{2r_{i-1/2}}$. The horizontal and vertical components of the total Darcy velocity at time t_n are approximated by $v_{i+1/2,j}^n$ and $v_{i,j+1/2}^n$.
The construction of S_{ij}^n, $S_{M_r j}^n$, S_{i1}^n and $S_{iM_z}^n$ has to be chosen differently in order to incorporate boundary conditions, which results into equations analogous to (23) and (24).
The second equation of (33) and the corresponding equations for the unknowns near the boundaries are a linear system of equations with a pentadiagonal coefficient matrix. Since this sparse matrix is symmetric positive definite, it can be solved efficiently by a preconditioned conjugate gradient method (see [10]).
As a possible improvement of the Godunov scheme we can consider a multi-dimensional version of the high resolution scheme. However, the construction of piecewise linear approximations for the saturation is not straightforward. These approximations have to be chosen such that the resulting scheme is conservative, which cannot be realised easily in combination with the use of exponential cylindrical coordinates.

4.2.2 A finite volume method for the pressure equation

In order to solve (33) an approximation for the total Darcy velocity $\mathbf{v}_t$ at time t_n needs to be available. Therefore the pressure equation (26) has to be solved for a given approximation for the saturation S. A conservative scheme can be constructed using the finite volume method (see [7]). Denote $\lambda^+(S) = \lambda_a(S) + \lambda_w(1-S)$ and $\lambda^-(S) = \lambda_a(S) - \lambda_w(1-S)$, then we obtain the scheme

$$\Delta z\left[R_{i+1/2}v_{i+1/2,j}^n - R_{i-1/2}v_{i-1/2,j}^n\right] + \Delta R_i^2\left[v_{i,j+1/2}^n - v_{i,j-1/2}^n\right] = 0,$$

where the horizontal and vertical components of the Darcy velocity at time t_n are approximated by

$$v^n_{i+1/2,j} = -\frac{1}{\Delta R_{i+1/2}}\left[\lambda^+(S^n_{i+1/2,j})(p^n_{i+1,j} - p^n_{ij}) + \lambda^-(S^n_{i+1/2,j})\frac{p_c(S^n_{i+1,j}) - p_c(S^n_{ij})}{2}\right],$$

$$v^n_{i,j+1/2} = -\frac{1}{\Delta z}\left[\lambda^+(S^n_{i,j+1/2})(p^n_{i,j+1} - p^n_{ij}) + \lambda^-(S^n_{i,j+1/2})\frac{p_c(S^n_{i,j+1}) - p_c(S^n_{ij})}{2}\right]$$
$$-(\rho_a\lambda_a(S^n_{i,j+1/2}) + \rho_w\lambda_w(1 - S^n_{i,j+1/2}))g.$$

The construction of $v^n_{1/2,j}$, $v^n_{M_r+1/2,j}$, $v^n_{i,1/2}$ and $v^n_{i,M_z+1/2}$ has to be chosen differently in order to incorporate boundary conditions. For the inner boundary $r = r_{in}$ this means that $v^n_{1/2,j} = v_{in}$ if $-h_l < z_j < -h_u$ and $v^n_{1/2,j} = 0$ otherwise. For the no-flow boundaries $r = r_{out}$ and $z = -h_b$ this respectively means that $v^n_{M_r+1/2,j} = 0$ and $v^n_{i,1/2} = 0$. For the top boundary it follows from (29) and (30) that

$$v^n_{i,M_z+1/2} = -\frac{1}{\Delta z}\left[\lambda^+(S^n_{iM_z})\left(-\frac{\rho_a + \rho_w}{2}g(h_t + \Delta z) - p^n_{iM_z}\right)\right]$$
$$-(\rho_a\lambda_a(S^n_{iM_z}) + \rho_w\lambda_w(1 - S^n_{iM_z}))g.$$

Again, the result is a linear system of equations with a symmetric pentadiagonal coefficient matrix, which can be solved efficiently by a preconditioned conjugate gradient method.

4.2.3 Numerical experiments

We consider (25)–(26) together with the boundary conditions (27)–(32). Let $h_t = 4$ m, $h_b = 6$ m, $h_u = 3$ m, $h_l = 4$ m, $r_{in} = \log 0.05$ and $r_{out} = 0$. The injection rate is equal to $Q = 5$ m^3 h^{-1}, which corresponds to $v_{in} \approx 4.421$ mm s^{-1}. The other relevant parameters are chosen as listed at the end of this article. We consider the solution at time $t = 240$ s. The domain $[r_{in}, r_{out}]\times[-h_b, h_t]$ is divided into M^2 cells of equal size $\Delta r\Delta z$. Time-sampling takes place at $t_n = n\Delta t$, $n = 0, 1, \ldots, N$, where $\Delta t = t/N$ is the time step. It is not clear which CFL-condition should hold, thus the time step is chosen such that $0 \le S^n_{ij} \le 1$. The results are displayed in Figure 11. Contour lines are plotted for $S = 0.05, 0.10, \ldots, 0.95$.
The linear systems resulting from the discretisation of the saturation and pressure equation are solved by the preconditioned conjugate gradient method with the zero fill-in incomplete Cholesky factorisation as a preconditioner (see [10]). For the saturation equation one iteration appeared to be sufficient. This suggests that the capillary pressure term in the saturation equation can be omitted, i.e. solving the hyperbolic problem can give sufficiently accurate results. However, in the one-dimensional case this results in a notably less accurate representation of the unsaturated zone.
For the pressure equation tens of iterations of the preconditioned conjugate gradient method have to be executed. This, in combination with the small time-step, makes the computation pretty expensive. Since the pressure field evolutes more slowly than the saturation field, a more efficient method can result from choosing a larger time-step for the pressure equation than for the saturation equation. Indeed, computing the pressure equation after 10 time-steps results in a proper approximation of the saturation (see Figure 12).

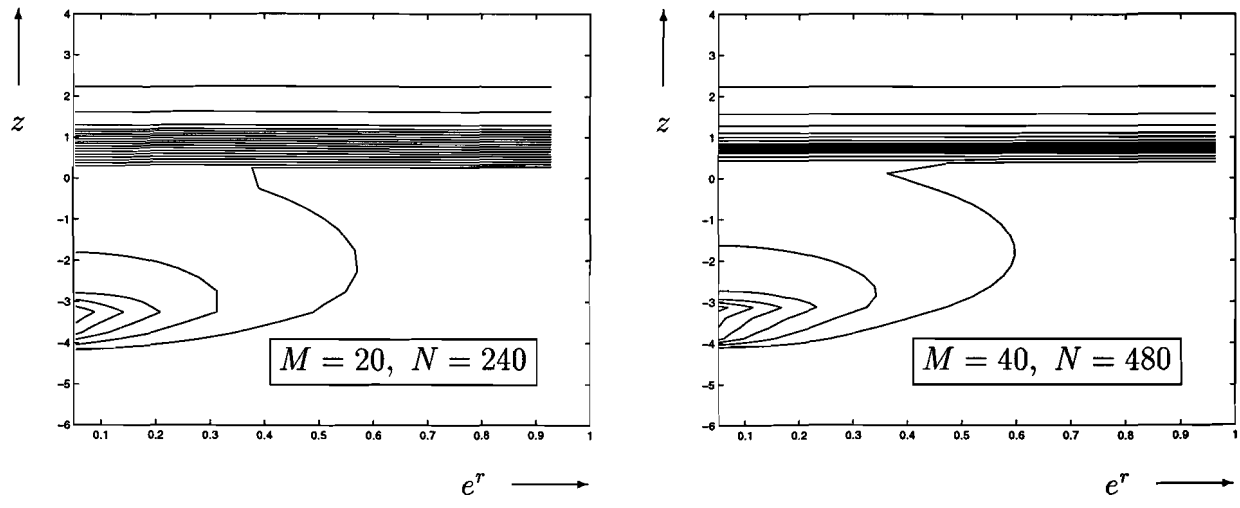

Figure 11: Solution for injection problem

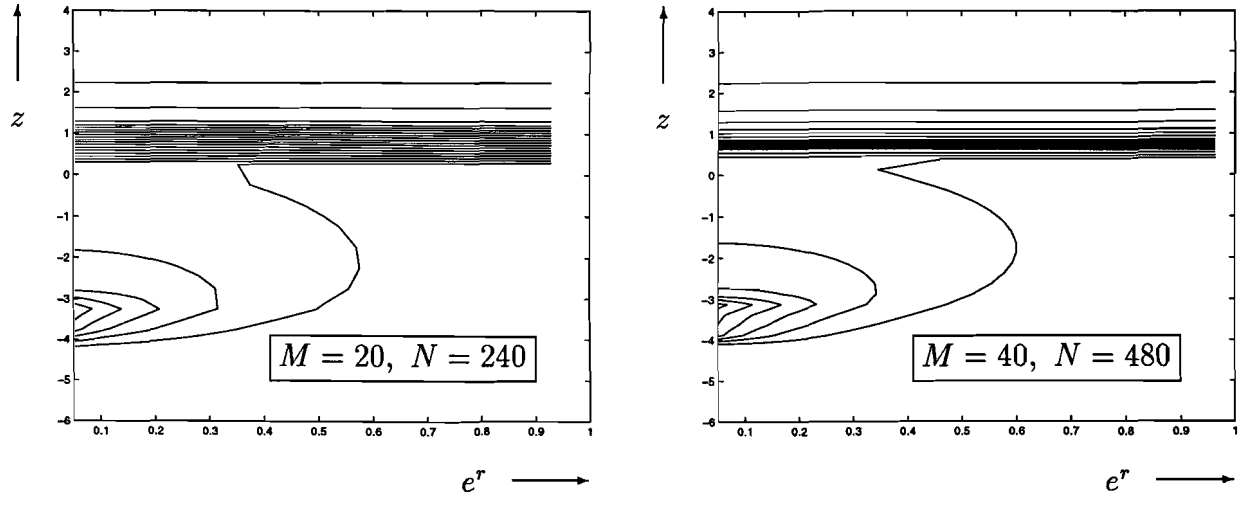

Figure 12: Solution for injection problem (pressure is computed after 10 time-steps)

5 Conclusions

In this study a conceptual model was constructed to simulate the physics of air sparging. It was argued that, under normal air sparging circumstances, this flow is predominantly driven by convection, so that the fractional flow model formulation is appropriate. One of the attractive features of the fractional flow approach is that the saturation equation can be solved efficiently.

Simulations were carried out for a one-dimensional and a multi-dimensional case. The modified Godunov scheme for the numerical approximation of the saturation performed satisfactorily. In the one-dimensional case a high resolution scheme gives slightly better results. However, generalising this scheme to more dimensions is not straightforward.

As usual, additional research can be executed. The accuracy and efficiency of the numerical solution of the fractional flow model and the mixed form of the Richards equation (see [2]) should be evaluated. Furthermore, the applicability of the model could be extended by including heterogeneity of the porous medium or air compressibility.

Nomenclature and parameter default values

symbol	meaning	parameter default value	unit
a	air phase (indicator)		
CFL	Courant number		–
D	capillary diffusion function		$m^2\ s^{-1}$
$\mathbf{e}_z$	unit vector in the positive z-direction		–
$\mathbf{F}$	flux function (vector)		$m\ s^{-1}$
F	flux function (scalar)		$m\ s^{-1}$
f_a	air fractional flow function		–
g	acceleration due to gravity	9.81	$m\ s^{-2}$
h	distance between boundary and initial water table		m
i	horizontal space index		
j	vertical space index		
$\mathbf{K}$	absolute permeability (tensor)		m^2
K	absolute permeability (scalar)	$5.3 \cdot 10^{-11}$	m^2
k_l	relative permeability of phase l		–
l	phase indicator, either a (air) or w (water)		
M	number of grid cells		
m	Van Genuchten soil constant	2/3	–
N	number of time-steps		
n	time level index		
p	average fluid pressure		Pa
p_l	pressure of phase l		Pa
p_c	capillary pressure		Pa
Q	air injection rate	5	$m^3\ h^{-1}$
r	exponential horizontal coordinate		
S_l	saturation of phase l		–
$S_{\mathcal{R}}$	solution of Riemann problem		–
S_r	residual water saturation		–
t	time		s
TV	total variation		
$\mathbf{v}_l$	Darcy velocity of phase l (vector)		$m\ s^{-1}$
$\mathbf{v}_t$	total Darcy velocity (vector)		$m\ s^{-1}$
v_t	total Darcy velocity (scalar)		$m\ s^{-1}$
v_{in}	Darcy injection flux in the air phase	$2.93 \cdot 10^{-4}$	$m\ s^{-1}$
w	water phase (indicator)		
z	vertical coordinate		m

symbol	meaning	parameter default value	unit
α	Van Genuchten soil parameter	2	m^{-1}
Δr	exponential cell width in horizontal direction		
Δt	time step		s
Δz	cell width in vertical direction		m
θ	cylindrical angle		–
λ	mobility function		$m^2\ Pa^{-1}\ s^{-1}$
λ_l	mobility of phase l		$m^2\ Pa^{-1}\ s^{-1}$
μ_a	viscosity of the air phase	$1.77 \cdot 10^{-5}$	Pa s
μ_w	viscosity of the water phase	$1.30 \cdot 10^{-3}$	Pa s
ρ_a	density of the air phase	1.24	$kg\ m^{-3}$
ρ_w	density of the water phase	$1 \cdot 10^3$	$kg\ m^{-3}$
σ	slope		–
ϕ	porosity	0.39	–

References

[1] A.C. BERKENBOSCH, E.F. KAASSCHIETER and J.H.M. TEN THIJE BOONKKAMP, *Finite-difference methods for one-dimensional hyperbolic conservation laws*, Numerical Methods for Partial Differential Equations **10** (1994), pp. 225–269

[2] M.I.J. VAN DIJKE, S.E.A.T.M. VAN DER ZEE and C.J. VAN DUIJN, *Multi-phase flow modelling of air sparging*, Advances in Water Resources **18** (1995), pp. 319–333

[3] M.TH. VAN GENUCHTEN, *A closed form equation for predicting the hydraulic conductivity of unsaturated soils*, Soil Science Society **44** (1980), pp. 892–898

[4] E. GODLEWSKI and P.-A. RAVIART, *Hyperbolic Systems of Conservation Laws*, Ellipses, Paris (1991)

[5] E. GODLEWSKI and P.-A. RAVIART, *Numerical Approximation of Hyperbolic Systems of Conservation Laws*, Springer, New York (1996)

[6] R.E. HINCHEE, R.N. MILLER and P.C. JOHNSON, *In Situ Aeration: Air Sparging, Bioventing, and Related Remediation Processes*, Battelle Press, Columbus (1995)

[7] C. HIRSCH, *Numerical Computation of Internal and External Flows*, Wiley, Chichester (1990)

[8] R.J. LEVEQUE, *Numerical Methods for Conservation Laws*, Birkhäuser Verlag, Basel (1990)

[9] M.C. MARLEY and F. LI, *Air sparging: an efficient groundwater and soils remediation technique*, in: R.E. Hinchee (eds.), *Air Sparging for Site Remediation*, Battelle Press, Columbus (1994), pp. 23–37.

[10] Y. SAAD, *Iterative Methods for Sparse Linear Systems*, PWS, Boston (1996).

PREVIOUS PUBLICATIONS IN THIS SERIES:

Number	Author(s)	Title	Month
97 03	J.J.A.M. Brands	Asymptotics of non-Laplacian integrals	February '97
97 04	M.J. Noot A.C. Telea J.K.M. Jansen R.M.M. Mattheij	Real Time Numerical Simulation and Visualization of Electrochemical Drilling	March '97
97 05	H.J.C. Huijberts	Characterization of static feedback realizable transfer functions for non-linear control systems	May '97
97 06	B. van 't Hof	Numerical Simulation of Unsteady Premixed Laminar Flames	July '97
97 07	P.W.C. Vosbeek J.H.G.M. van Geffen V.V. Meleshko G.J.F. van Heijst	Collapse interactions of finite-sized two-dimensional vortices	July '97
97 08	T.D. Chandra S.W. Rienstra	Analytical Approximations to the Viscous Glass Flow Problem in the Mould-Plunger Pressing Process	August '97
97 09	C. Bahriawati S.W. Rienstra	The dynamics of a suspended pipeline in the limit of vanishing stiffness	August '97
97 10	A.F.M. ter Elst D.W. Robinson	Local lower bounds on heat kernels	August '97
97 11	E.F. Kaasschieter J.D. van der Werff ten Bosch G.J. Mulder	A Numerical Fractional Flow Model for Air Sparging	September '97